HSF-1 promotes longevity through ubiquilin-1 dependent mitochondrial network remodelling

Johnathan Labbadia (✉ j.labbadia@ucl.ac.uk)
University College London https://orcid.org/0000-0001-9625-2816
Annmary Erinjeri
UCL https://orcid.org/0000-0002-1427-5342
Xunyan Wang
UCL
Rhianna Williams
UCL
Riccardo Zenezini Chiozzi
Utrecht University
Konstantinos Thalassinos
University College London https://orcid.org/0000-0001-5072-8428

Article

Keywords:

Posted Date: November 3rd, 2023

DOI: https://doi.org/10.21203/rs.3.rs-3481052/v1

Additional Declarations: There is **NO** Competing Interest.

Abstract

Increased activity of the heat shock factor, HSF-1, suppresses proteotoxicity and enhances longevity. However, the precise mechanisms by which HSF-1 promotes lifespan are unclear. Using an RNAi screen, we have identified ubiquilin-1 *(ubql-1)* as an essential mediator of lifespan extension in worms overexpressing *hsf-1*. We find that *hsf-1* overexpression leads to transcriptional downregulation of all components of the CDC-48-UFD-1-NPL-4 complex, which is central to both endoplasmic reticulum and mitochondria associated protein degradation, and that this is complemented by UBQL-1-dependent turnover of NPL-4.1. As a consequence, mitochondria undergo extensive remodelling, leading to metabolic rewiring and increased lifespan. Together, our data are the first to establish that HSF-1 mediates lifespan extension through mitochondrial network adaptations that occur in response to the down-tuning of organellar protein degradation pathways.

Main Text

Ageing is a major risk factor for chronic morbidities such as cancers, cardiovascular disorders, and neurodegeneration. These diseases contribute to a rising burden on families, communities, and healthcare across the world. Environmental and genetic factors contribute to ageing by influencing a complex network of pathways and processes that drive cellular dysfunction [1]. These include the loss of protein homeostasis (proteostasis), which is characterised by the appearance and aggregation of misfolded and mislocalised proteins within cells and tissues [2].

Cells possess an array of protein quality control mechanisms collectively referred to as the proteostasis network (PN), which act to preserve proteome integrity. The PN coordinates protein synthesis, folding, disaggregation and degradation and integrates components of the translational machinery, molecular chaperones and co-chaperones and the proteolytic systems - the ubiquitin–proteasome system (UPS), and autophagy-lysosomal system - to ensure cell viability [3].

The cytosolic/nuclear arm of the PN is subject to regulation by heat shock transcription factor 1 (HSF-1), which protects the proteome by driving the expression of heat shock proteins (HSPs) that function as molecular chaperones [3,4]. In line with its function, knock down of HSF-1 leads to increased protein aggregation, tissue dysfunction and decreased survival, whereas overexpression of HSF-1 maintains proteome integrity, promotes tissue health, and extends lifespan. While it is apparent that increasing HSF-1 activity is beneficial for longevity, our understanding of the mechanisms that act downstream of HSF-1 to prolong healthy tissue function, remains limited.

It is widely believed that HSF-1 regulates ageing by upregulating the expression of HSPs. However, in addition to HSPs, HSF-1 also controls the expression of genes encoding cytoskeletal components, metabolic enzymes, ribosomal subunits, chromatin factors and components of the UPS [5,6]. Moreover, recent work has demonstrated roles for autophagy [7], maintenance of the cytoskeleton and lipid

regulation [8,9] in HSF-1 mediated lifespan extension. These observations indicate that HSF-1 regulates longevity through mechanisms beyond HSP mediated chaperoning of the proteome.

Here, we employed an RNAi screen to identify the HSF-1 target genes that promote increased lifespan in *C. elegans* over expressing HSF-1 (*hsf-1* OE). We have found that the sole worm ubiquilin, ubiquilin-1 (*ubql-1*), is necessary for *hsf-1* OE to increase lifespan. Ubiquilins are multifaceted, conserved shuttle proteins that localise to the cytoplasm and nucleus [10] where they function as chaperones that aid in the degradation of substrates through the ubiquitin-proteasome system and autophagy. This is facilitated by their N-terminal Ubiquitin (Ub)-like (UBL) domain and C-terminal Ub-associated (UBA) domain, which enable binding to the proteasome and polyubiquitinated chains [11].

Despite its central role in protein degradation, we find that ubiquilin-1 does not promote longevity by altering general proteostasis capacity. Instead, ubiquilin-1 increases lifespan upon overexpression of HSF-1 by promoting a reduction in organellar protein degradation, mitochondrial network remodelling and metabolic rewiring.

Ubiquilin-1 is required for HSF-1 mediated lifespan extension

Overexpression of HSF-1 (*hsf-1* OE) leads to extension of lifespan in *C. elegans* [9,12,13]. To better understand the mechanisms that act downstream of HSF-1 to promote longevity, an RNAi screen was performed to determine which HSF-1 target genes are required for the increased lifespan of *hsf-1* OE worms. Our RNAi screen consisted of 96 *C. elegans* genes shown to be directly regulated by HSF-1 under basal or stress conditions (Supplementary Fig. 1a and Supplementary Table 1) [14]. We identified the gene ubiquilin-1 (*ubql-1*) as the strongest modifier of *hsf-1* OE lifespan, without comparable effects on the lifespan of wildtype worms (Fig. 1a). Consistent with previous reports that *ubql-1* is bound by HSF-1 (Supplementary Fig. 1b), *hsf-1* OE worms exhibited increased *ubql-1* expression in early adulthood (Fig. 1b).

To verify our RNAi screen, we grew animals on empty vector control (L4440) or *ubql-1*(RNAi) and measured survival in two independent *hsf-1* OE lines. Knockdown of *ubql-1* suppressed the increased lifespan of both *hsf-1* OE lines tested (Fig. 1c and Supplementary Fig. 1d). In addition, we also assessed lifespan in *ubql-1(tm1574)* mutants that harbour a 755bp deletion spanning the whole of exons 1 and 2, and express reduced levels of a truncated *ubql-1* mRNA (Fig. 1b, Supplementary Fig. 1c and Supplementary Fig. 1e). Lifespan assays revealed that *ubql-1(tm1574)* mutants are shorter lived than wildtype controls and that the presence of the *ubql-1(tm1574)* mutation reduces the lifespan of *hsf-1* OE worms to that of wildtype animals (Fig. 1d). Together our data establish UBQL-1 as a mediator of HSF-1 mediated longevity extension in *C. elegans*. Therefore, we sought to investigate the processes through which UBQL-1 impacts longevity.

Maintenance of proteostasis capacity does not require ubql-1 function

To better understand the mechanisms by which *ubql-1* functions to supress ageing downstream of HSF-1, we first investigated whether ubiquilin-1 influences HSF-1 activity. Loss of *ubql-1* function did not suppress the expression of canonical HSF-1 target genes (*hsp-16.11* or *hsp-70*) basally, or in response to heat shock, in wildtype or *hsf-1* OE worms (Fig. 2a-b and Supplementary Fig. 2a-b), demonstrating that HSF-1 activity is unaffected by the loss of *ubql-1* activity.

Next, we asked whether *ubql-1* is necessary for worms to manage heat induced protein folding stress. As expected, *hsf-1* OE worms survived for longer than wildtype worms following heat stress as young adults (Fig. 2c). Despite being shorter lived, *ubql-1* mutants were more stress resistant than wildtype worms; however, stress resistance was not further increased in *ubql-1* mutants upon overexpression of HSF-1 (Fig. 2c). Given that *ubql-1* mutants do not exhibit increased HSF-1 activity, these data suggest that *ubql-1* is necessary for increased stress resistance in *hsf-1* OE worms.

Many factors and pathways can contribute to stress resistance. Therefore, to more precisely examine the effects of *ubql-1* on proteostasis capacity, we took advantage of well-described polyglutamine::YFP-based (PolyQ::YFP) proteostasis sensors [15,16] expressed exclusively in the intestine (Q44) or body wall muscles (Q35). PolyQ aggregation increased with age in both intestinal and muscle tissues (Fig. 2d-f and Supplementary Fig. 2c-e) of wildtype worms. PolyQ aggregation was strongly suppressed on day 3 and day 5 of adulthood in worms overexpressing HSF-1 (Fig. 2d-f and Supplementary Fig. 2c-e). Surprisingly, *ubql-1*(RNAi) did not alter the aggregation of polyQ proteins in the intestine or muscles (Fig. 2d-f and Supplementary Fig. 2c-e) and did not prevent *hsf-1* OE from suppressing polyQ aggregation in these tissues compared to wildtype counterparts (Fig. 2d-f and Supplementary Fig. 2c-e). Taken together, these data indicate that UBQL-1 does not influence longevity in *hsf-1* OE worms by broadly promoting proteostasis capacity.

Ubiquilin-1 promotes metabolic remodelling in hsf-1 OE animals

To ascertain how *ubql-1* promotes longevity, we employed transcriptomics and proteomics to identify genes, proteins and pathways that are altered in *hsf-1* OE worms in a UBQL-1 dependent manner. Increased HSF-1 activity generated substantial changes across both the proteome and transcriptome with a total of 1,564 proteins (948 increased and 616 decreased) and 3,262 transcripts (2,343 increased and 919 decreased) altered compared to wildtype worms (Fig. 3a, Supplementary Fig. 3a, Supplementary Table 3 and Supplementary Table 4). While we did not observe a strong overlap in the specific identities of altered proteins and genes across our proteomic and transcriptomic datasets (Supplementary Fig. 3b), there was a good functional correlation between the two datasets, with KEGG analysis [17] revealing that up-regulated genes and proteins were enriched for pathways regulating metabolism and protein processing in the endoplasmic reticulum (ER), while down-regulated genes and proteins were enriched for pathways that included mismatch repair, DNA replication and signalling pathways (Fig. 3b and Supplementary Fig. 3c).

Loss of *ubql-1* function in wildtype worms resulted in altered abundance (FDR $p < 0.05$) of 68 proteins, of which, 43 were increased, and 25 were decreased (Supplementary Fig. 3d, Supplementary Table 3). Similarly, RNA-seq analysis revealed that *ubql-1(tm1574)* mutants exhibited 402 up-regulated and 16 down-regulated (Log 2-FC, FDR $p < 0.05$) genes compared to wildtype worms (Supplementary Fig. 3e, Supplementary Table 4). Of the proteomic and transcriptomic changes observed in *hsf-1* OE worms, 12 proteins and 61 genes were increased in a *ubql-1* dependent manner, and 4 proteins and 17 genes were down-regulated in a *ubql-1* dependent manner (Fig. 3c-f and Supplementary Fig. 3f). Interestingly, many *ubql-1* dependent genes had roles in lipid metabolism (Fig. 3f) and UBQL-1 has been shown to interact strongly with the central metabolic regulator, NHR-49 [18].

Among the proteins whose levels were reduced in *hsf-1* OE worms lacking a fully functional UBQL-1, was the acyl-CoA synthetase-2 (ACS-2), a key enzyme in mitochondrial beta-fatty acid oxidation that is known to localise to mitochondria [19–21] (Fig. 3d). ACS-2 levels are controlled by NHR-49, which has been shown to be necessary for lipid homeostasis and increased lifespan in *hsf-1* OE worms [8,19–23]. Furthermore, five of the other 11 proteins regulated in *hsf-1 OE* animals by UBQL-1 (UMPS-1, PGP-6, IRG-1, SEU-1, and CRML-1*)* have been shown to associate with NHR-49 (Fig. 3d and Supplementary Fig. 3g), with only *irg-1* and *pgp-6* exhibiting concomitant changes in transcription (Fig. 3f). Moreover, exposure to *nhr-49*(RNAi) shortened lifespan across all backgrounds tested, with the loss of either NHR-49 or UBQL-1 suppressing *hsf-1* OE lifespan to a similar extent, with no additive effect observed (Supplementary Fig. 3h and i). Taken together, our data suggest that the increased lifespan of *hsf-1* OE worms is mediated by UBQL-1 dependent metabolic remodelling, at least in part, through NHR-49 activity, possibly by altering the stability of NHR-49 complexes.

Ubiquilin-1 promotes down-tuning of endoplasmic reticulum and mitochondrial associated degradation components in hsf-1 OE animals

Ubiquilins have a central role in protein degradation pathways associated with the cytosol/nucleus, endoplasmic reticulum (ER) and mitochondria [11,24–26]. Therefore, we reasoned that UBQL-1 promotes metabolic remodelling and lifespan extension in *hsf-1* OE animals by promoting the degradation of key target proteins. Therefore, we focused our attention on proteins whose levels were elevated in *hsf-1 OE* animals upon reduction of UBQL-1 function.

Among the proteins whose levels are decreased upon *hsf-1* OE, we identified 4 whose reduction was dependent on UBQL-1. Among these, the protein NPL-4.1 displayed the strongest increase in abundance in *ubql-1* mutant animals (Fig. 3d). NPL-4.1 is a central component of the CDC-48-NPL-4-UFD complex, which is at the core of both ER associated protein degradation (ERAD) and mitochondria associated protein degradation (MAD)[27], suggesting that the reduced activity of these pathways may be linked to lifespan extension in *hsf-1* OE worms. Consistent with this, we also observed a strong reduction in *npl-4.1, npl-4.2, ufd-1, cdc-48.1 and cdc-48.2* mRNA levels in *hsf-1* OE worms compared to wild type animals, although transcript levels were not restored in *ubql-1* mutants (Supplementary Fig. 4a). Consistent with a reduction in ERAD, we observed that “protein processing in the ER” was the strongest enriched term

among our set of increased proteins in *hsf-1* OE worms (Fig. 3b) and that *hsf-1* OE worms were highly sensitive to ER stress induced by tunicamycin (Supplementary Fig. 4b). While we did not observe evidence for activation of the UPR^{mt} (Supplementary Fig. 4d-e), we did find that, consistent with a reduction in MAD, mitochondrial network organisation was dramatically altered upon *hsf-1* OE [28] (Supplementary Fig. 4c). Together, these observations suggest that a mild impairment of organellar protein degradation is associated with the increased lifespan of *hsf-1* OE worms.

To determine how gross defects in ERAD or MAD impact lifespan in *hsf-1* OE or wild type worms, we used RNAi to knock-down the E3 ligase, SEL-11/HRD-1 (which is necessary for ERAD), or individual components of the CDC-48-NPL-4-UFD-1 complex. Knockdown of *sel-11* reduced lifespan to a comparable extent in both wildtype and *hsf-1* OE worms, suggesting that ERAD is required for normal lifespan but does not interact with *hsf-1* OE to influence lifespan (Fig. 4a). In contrast, while knockdown of *npl-4.1/4.2, ufd-1* or *cdc-48.1* was detrimental to all genotypes tested, knockdown of any of these factors inverted the lifespans of wildtype and *hsf-1* OE worms (Fig. 4b-d). While these effects were not suppressed by loss of UBQL-1 function, this is likely because UBQL-1 activity becomes critical for the removal of toxic proteins that build up upon severe loss of the CDC-48-UFD-1-NPL-4 complex.

Together, these data suggest that increased HSF-1 expression compromises organellar protein degradation pathways, leading to a mitochondrial network adaptation that results in a more fused mitochondrial network and altered metabolic homeostasis.

HSF-1 overexpression promotes lifespan by altering mitochondrial dynamics

To shed light on whether UBQL-1 is necessary for changes in mitochondrial function and network dynamics upon *hsf-1* OE, we first assessed respiration rates, total ATP-levels and lipid stores (measured by Oil-Red-O staining [29]) across our four genotypes. Overexpression of *hsf-1* reduced oxygen consumption rates (OCR) and increased mitochondrial fusion in a *ubql-1* dependent manner but did not alter ATP levels or total trigylceride levels (Fig. 5a-c and Supplementary Fig. 5a-f). However, we did observe a comparable reduction in lipid stores upon loss of UBQL-1 function in wildtype and *hsf-1* OE worms (Supplementary Fig. 5b and c), suggesting a previously undiscovered role for ubiquilins in lipid homeostasis.

Mitochondrial metabolic capacity is linked to network morphology [30] and NHR-49 is known to be important for mitochondrial dynamics [23]. Maintenance of mitochondrial networks is controlled via fission and fusion [31,32], therefore, to test whether mitochondrial network dynamics are important for the extended lifespan of *hsf-1* OE worms, we measured survival in worms in which core fusion/fission mediators were targeted by RNAi, specifically, the cytosolic dynamin-like GTPase DRP-1 [33] and the membrane-anchored dynamin-like GTPases FZO-1/mitofusin [34] and EAT-3/OPA1 [35].

RNAi against *fzo-1* or *eat-3* extended lifespan in wildtype worms to a level comparable to that seen upon *hsf-1* OE (Fig. 5d and e). However, no additive effect on lifespan was observed in *hsf-1* OE; *fzo-1*(RNAi) or

eat-3(RNAi) groups (Fig. 5d and e). In contrast, *drp-1*(RNAi) only modestly increased lifespan in wildtype animals and strongly suppressed lifespan extension upon *hsf-1* OE (Fig. 5f). Given that mitochondrial fission contributes to mitochondrial homeostasis by segregating damaged mitochondria for degradation via mitophagy [36], we investigated whether mitophagy is also necessary for the elevated lifespan of *hsf-1* OE worms. Knockdown of the kinase PINK-1 (a core mitophagy inducer) did not suppress lifespan extension in *hsf-1* OE worms (Supplementary Fig. 5g) and mitochondrial copy number was unaltered by *hsf-1* OE or *ubql-1* mutation (Supplementary Fig. 5h). Together, our data show that in response to *hsf-1* overexpression, UBQL-1-mediated changes in mitochondrial network dynamics promote longevity independently of mitophagy or UPR^{mt} activation. Furthermore, our findings reveal that the longevity promoting effects conferred by *hsf-1* OE stem from mitochondrial network adaptations in response to reduced organellar protein degradation.

Discussion

Our work identifies UBQL-1 as a key determinant of the extended longevity conferred by over expression of HSF-1. Research in yeast and mammalian cells has shown that ubiquilin proteins localise to the nucleus and cytoplasm and function in protein degradation pathways [10,11,37] by acting as shuttle proteins that transport ubiquitinated substrates to both the proteasome and the autophagy-lysosomal systems [38]. Ubiquilins are also known components of ERAD complexes [39] and knockdown of *ubql-1* in worms leads to induction of the ER unfolded protein response and the accumulation of misfolded proteins [25,40]. UBQLN1 has also previously been linked to maintenance of mitochondrial protein homeostasis, with studies showing that UBQLN1 targets mislocalized mitochondrial outer membrane proteins for proteasomal degradation. In addition, UBQLN1-deficient cells accumulate mislocalized mitochondrial proteins in the cytosol, leading to a loss in viability [24,26]. It is perhaps surprising then that we did not identify a greater number of proteins exhibiting altered abundance in wildtype or *hsf-1* OE worms upon removal of UBQL-1. One possible explanation for this is that there may be residual UBQL-1 activity remaining in our mutant strain. Alternatively, UBQL-1 may only be critical for the turnover of a limited sub-set of proteins or the activity of other pathways, such as the autophagy lysosome system, may be increased to compensate for the loss of UBQL-1.

Nevertheless, we were able to identify key proteins whose abundance was altered upon loss of UBQL-1 function, including the mitochondrial acetyl CoA-synthetase, ACS-2, and the NPL-4.1 subunit of the CDC-48 complex. Our finding that ubiquilin-1 promotes the long lifespan of *hsf-1* OE animals by facilitating mitochondrial fusion and reduced oxidative phosphorylation rather than broadly altering proteostasis capacity was surprising, but also consistent with recent published and non peer-reviewed observations from other groups. Specifically, increased HSF-1 activity and extended lifespan in *hsb-1* mutants has been linked to activation of the UPR^{mt} and altered mitochondrial homeostasis in *C. elegans* [41]. Furthermore, altered lipid homeostasis and NHR-49 activity have been linked to increased lifespan in *C. elegans* overexpressing *hsf-1* [6,8,18,42,43] and NHR-49 has been shown to mediate increased HSF-1 activity,

enhanced stress resistance and augmented proteostasis capacity in germline stem cell deficient worms [42].

In *C. elegans*, NHR-49 is required for normal lifespan by functioning with its coactivator, the mediator subunit MDT-15, and the NHR co-factors, NHR-13/-22/-80/-66/-105, to influence metabolism and mitochondrial function [19,23]. It is unclear whether UBQL-1 promotes NHR-49 activity directly, as a consequence of alterations in MAD, or both [18]. In addition, it is possible that the HSF-1-UBQL-1 axis may also converge on lysosomal function, which has been shown to be critical for maintaining cellular homeostasis and tissue health [44] via NHR-49 [45,46]. Consistent with this, we observe that several lysosomal genes are up-regulated in worms over-expressing HSF-1, including those previously considered essential to extended lifespan [47]. However, our data point towards increased NHR-49 activity and metabolic remodelling occurring downstream of alterations in mitochondrial homeostasis due to impaired MAD.

We observed that UBQL-1 promotes changes in mitochondrial network structure in *hsf-1* OE worms. Furthermore, manipulating either fission or fusion prevents *hsf-1* OE from extending lifespan, indicating that a shift in the balance of mitochondrial network homeostasis is more important for lifespan than specifically driving mitochondria towards a more fused or fragmented state [48]. This is consistent with similar reports regarding the interplay between mitochondrial networks and increased lifespan upon dietary restriction. The fact that worms overexpressing HSF-1 have low basal respiration despite a more fused mitochondrial network was unexpected, as mitochondrial fusion has previously been linked to higher OCR in mammalian cells[49–51]. However, studies in flies have indicated that morphology and function of mitochondria can be dissociated[52]. Alternatively, it may be that a more longitudinal investigation of OCR and mitochondrial dynamics will reveal that OCR is restored or increased in *hsf-1* OE animals later in life. Understanding the precise nature of this relationship will help unravel the specific events that lead to lifespan extension when HSF-1 activity is increased.

Finally, while beyond the scope of this study to explore, it is also possible that the effects of ubiquilin-1 on mitochondria stem from interactions with the cytoskeleton. Ubiquilin-1 is important for cytoskeleton organisation in cancer cells [53] and we observed that RHO GTPase-activating proteins, namely *rga-3* (K09H11.3) and *crml-1*, were increased in *hsf-1* OE worms in a *ubql-1* dependent manner. RHO GTPases have roles in actin cytoskeleton organisation [54], the maintenance of which has been shown to be modulated by HSF-1 in regulating aging and stress resistance [9,55]. In yeast it is known that organisation of the cytoskeleton impacts mitochondrial quality control [9,55–57] and that mitochondrial dynamics are modulated by cytoskeletal interactions [58–60]. Therefore, future experiments to understand the interplay between ubiquilin activity, mitochondrial fission–fusion dynamics, cytoskeletal integrity and ageing may help expand our understanding of how HSF-1 promotes longevity.

In summary, our work establishes an HSF-1-UBQL-1-Mitochondrial axis that promotes longevity by remodelling mitochondrial networks and rewiring metabolism in *C. elegans*. These findings challenge

existing assumptions and highlight mitochondrial dynamics as an additional component of HSF-1 mediated lifespan extension.

Materials and methods

C. elegans strains and culture conditions

All strains were maintained at 20˚ C on NGM plates seeded with *Escherichia coli* OP50 under standard conditions, ([61] unless mentioned otherwise. Strains used in this study were: N2 Bristol (wild type laboratory strain), JPL52 *ubql-1(tm1574)4x*, AGD710 *uthIs235 [sur-5p::hsf-1::unc-54 3'UTR + myo-2p::tdTomato::unc-54 3' UTR*] referred to as *hsf-1* OE in this manuscript, JPL54 - AGD710 crossed to JPL52, AM140 *(rmIs132 [unc-54p::Q*(35)::*YFP])*, JPL66 - AGD710 crossed to AM140, AM738 *(rmIs297 [vha-6p::Q*(44)::*YFP, rol-6(su1006)])*, JPL67 - AGD710 crossed to AM738, SJ4103 *zcls14 [myo-3::GFP(mit)]*, JPL84 - AGD710 crossed to SJ4103, AM583 *myo-2p::gfp; hsf-1*p::*hsf-1*

STRAIN	LAB NUMBER	GENOTYPE	SOURCE
Bristol N2	Bristol N2	N2(wild-type Bristol isolate)	CGC
FX01574	JPL52	*ubql-1(tm1574)4x*	NBRP, 4 times outcrossed to Bristol N2
AGD710	AGD710	*uthIs235 [sur-5p::hsf-1::unc-54 3'UTR + myo-2p::tdTomato::unc-54 3' UTR]*	CGC, referred to as *hsf-1* OE
-	JPL54	*hsf-1* OE;*ubql-1(tm1574)*	This study
AM583	AM583	*myo-2p::gfp; hsf-1*p::*hsf-1*	Morimoto Lab
AM140	AM140	*rmIs132 [unc-54p::Q(35)::YFP]*	CGC
-	JPL66	*hsf-1* OE; *rmIs132 [unc-54p::Q(35)::YFP]*	This study
AM738	AM738	*rmIs297 [vha-6p::Q(44)::YFP, rol-6(su1006)]*	Morimoto lab
-	JPL67	*hsf-1* OE;*vha-6p::Q(44)::YFP, rol-6(su1006)*	This study
SJ4103	SJ4103	*zcls14 [myo-3::GFP(mit)]*	CGC
-	JPL84	*hsf-1* OE; *zcls14 [myo-3::GFP(mit)]*	This study

RNA interference

All clones were sequenced verified before use and were obtained from the Ahringer RNAi library [62]. RNAi was initiated by growing bacteria for 16 hours at 37˚ C in LB containing 100 ug/ml ampicillin, with shaking (220 rpm). Cultures were then induced with 5 mM IPTG and allowed to grow at 37˚ C for a further 3 hours. After induction, bacteria were allowed to cool at room temperature and were then seeded onto

NGM RNAi plates containing 100 ug/ml ampicillin and 1 mM IPTG. Plates with seeded bacteria were allowed to dry at room temperature before use.

Lifespan, stress resistance and motility assays

Survival for lifespan and stress resistance assays was scored by gently touching/prodding worms with a platinum pick at the indicated time points. Worms were scored as dead when they stopped responding to prodding and in the absence of pharyngeal pumping. Censored worms in lifespan assays included exploded animals, those exhibiting bagging (internal hatching of progeny), rupturing through the vulva and worms that dried out on the edge of the plates and/or crawled off the plate. Motility assays were based on categorisation of their locomotory phenotypes [63]. These were Class A, worms exhibiting vigorous movement in response to touch; Class B, those that move only when prodded and leave non-sinusoidal tracks (uncoordinated movement); and Class C, worms that do not respond to prodding (no movement forwards or backwards) but do show head and/or tail movements or twitch in response to touch. The incidence of class C animals was plotted as paralysed worms in the paralysis assay. In stress resistance assays, worms were heat shocked on seeded NGM plates at 33˚ C for 4 hours and allowed to recover at 20˚ C. Censored worms in stress resistance assays were only those worms that dried out on the edge of the plates/crawled off the plate. For tunicamycin treatment, worms were transferred to seeded NGM plates containing tunicamycin (50 ug/ml) on day 1 of adulthood. Survival statistics for all experimental repeats can be found in Table S1.

Proteostasis sensor assays

Polyglutamine aggregation was scored in muscle and intestinal proteostasis sensors – AM140, JPL66, AM738, JPL67 grown on empty vector and *ubql-1*(RNAi) at indicated time points. For obtaining images and aggregate counting, worms were immobilised on 3% agar pads in 3mM levamisole and images were captured using a Zeiss Imager.Z2 microscope (10x) and Hamamatsu ORCA-Flash 4.0 digital CMOS camera. Aggregates were determined to be any discrete foci exhibiting fluorescence signal above the background diffuse signal.

RNA extraction, cDNA synthesis and RTqPCR

Approximately 100–200 adult animals per treatment group were lysed in 250 ul of Trizol by vortexing for 10 minutes at 4˚ C in three cycles. RNA was purified using an RNeasy extraction kit as per manufacturer's instructions. cDNA was generated using 1ug of total RNA and an iScript cDNA synthesis kit. Real-time quantitative PCR was performed using a Biorad CFX96 Real-time PCR detection system and BioRad SsoAdvanced SYBR green super mix. Expression of genes of interest was calculated relative to the housekeeping genes *pmp-3, rpb-2* and *cdc-42* using the standard curve method. Sequences for all primer pairs used in this study can be found in Table S5.

RNA-sequencing and analysis

RNA integrity was assessed using an RNA Nano 6000 assay kit and an Agilent Bioanalyzer 2100 system. Following this, mRNA was purified from 1 µg of total RNA using poly-dT magnetic beads and cDNA

libraries were generated using random hexamers and M-MuLV reverse transcriptase for first strand synthesis, followed by second strand synthesis using DNA polymerase I and RNase H. Fragments were blunt-ended and adapters were ligated before PCR was performed using Phusion high fidelity DNA polymerase. PCR products were purified using an AMPure XP system and library quality was checked using an Agilent Bioanalyzer 2100. Libraries were sequenced using an Illumina Novaseq 6000 platform to generate paired-end 150 base pair reads at a depth of 20 million reads per sample. Following sequencing, raw data was checked and reads containing adapter sequences, poly-N reads or poor-quality sequences were removed. Reads were then aligned to the *C. elegans* reference genome using Hisat2 v2.0.5 and featureCounts v1.5.0-p3 was used to quantify the number of reads mapped to each gene. Differential expression testing was carried out using DESeq2 and p-values were adjusted using Benjamini-Hochberg. Up or down regulated genes were analysed using the G:profiler [17] tool (biit.cs.ut.ee/gprofiler/gost) to identify KEGG processes/pathways that were enriched in the groups being compared. Volcano Plots were created using the web app, VolcaNoseR [64]. Raw and unprocessed data sets can be obtained through the Gene Expression Omnibus using accession number: GSE241558.

Oxygen consumption assays

Oxygen consumption rate (OCR) was measured in worms using the Seahorse XF96 (Seahorse Bioscience) as previously described [65]. In brief, wildtype, *ubql-1(tm1574)*, *hsf-1* OE and *hsf-1* OE;*ubql-1(tm1574)* animals were cultured on plates with OP50 bacteria and grown till Day 1(YA). On the day of analysis, Day 1(YA) worms were transferred from respective NGM plates to plates without food to remove bacteria. Next, worms were transferred in 96-well Seahorse plates (approximately 10 worms per well and 10 such wells per condition tested) and OCR was measured 8 times. FCCP and Sodium Azide treatments were done at a final well concentration of 10 mM and 40 mM respectively. Mitochondrial (basal) OCR were measured for each condition. Data was normalised to worms per well.

Mitochondrial morphology assays

For mitochondrial morphology imaging, the transgenic strains expressing GFP-tagged mitochondrial protein in the body wall muscles, *zcls14[myo-3::GFP(mit)]* strain and *hsf-1* OE;*zcls14[myo-3::GFP(mit)]* animals grown on empty vector and *ubql-1*(RNAi) were utilised. Worms were immobilised on 3% agar pads in 3mM levamisole and images were captured using a Zeiss Imager.Z2 microscope and Hamamatsu ORCA-Flash 4.0 digital CMOS camera (63x/1.40 oil objective lens) on Days 2 and 3 of adulthood. The region between the pharynx and vulva or the vulva and tail were selected for viewing muscle mitochondrial networks. Images were processed using ImageJ. Qualitative analysis of the mitochondria morphology was done, and images were scored as fused, tubular, intermediate or fragmented based on the mitochondrial network organization.

Oil Red O staining

Staining for lipid levels was essentially performed as previously described [29] Briefly, worms were washed 3 times in M9 buffer, fixed immediately in 60% isopropanol at room temperature, and then stained with freshly filtered ORO (60% ORO working solution) overnight at 25˚ C. Oil Red O solution was then washed-

out using M9-0.01% Triton-X and worms were mounted on 3% agarose pads. Images were acquired on a Nikon SMZ1270 stereo microscope with a DS-Fi3 5.9 MP colour camera. Images were processed using ImageJ.

ATP assays

Approximately 1000 wildtype, *ubql-1(tm1574)*, *hsf-1* OE and *hsf-1* OE;*ubql-1(tm1574)* animals were cultured on plates with OP50 bacteria and collected on Day 1 of adulthood (YA). Worm pellets were resuspended in 50ul RIPA buffer lysate and protein concentration in each sample was estimated using the PierceTM BCA Protein Assay Kit (Thermo Scientific) following the instructions of the manufacturer. ATP levels were quantified using a luciferin/luciferase-based ADP/ATP Ratio assay kit (Sigma Aldrich) as per manufacturer's instructions. Luminescence was then measured using a Tecan Infinite M200 microplate reader and levels of ATP were calculated.

Protein extraction and western blotting

To extract protein for western blotting, wildtype and *hsf-1* OE worms (approximately 1000) were collected in M9, pelleted, and then resuspended in RIPA buffer supplemented with a protease inhibitor cocktail tablet. Worm pellets were flash frozen in liquid nitrogen and crushed (4 cycles) in microcentrifuge tubes using a plastic dounce homogenizer. Lysates were then centrifuged at 13,000 rpm at 4˚ C for 15 minutes and the supernatant was collected. Protein concentration in each sample was estimated using the PierceTM BCA Protein Assay Kit (Thermo Scientific) following the instructions of the manufacturer. Proteins were separated by SDS-PAGE and transferred to nitrocellulose membranes before probing with primary antibodies. Blots were incubated with primary antibody for 1.5h at room temperature (HSP-6– 1:1000, α-tubulin − 1:10000), washed 3x with PBS-0.2% Tween, incubated with secondary antibodies for 1h at room temperature (rabbit-HRP – 1:5000, mouse-HRP – 1:5000), washed a further 3x with PBS-0.2% Tween, and then developed using ECL detection reagents and Odyssey XF Imager. Densitometry of protein bands was performed using ImageJ gel analysis tools.

Proteomics

Approximately 1000 wildtype, *ubql-1(tm1574)*, *hsf-1* OE and *hsf-1* OE;*ubql-1(tm1574)* animals were cultured on plates with OP50 bacteria and collected on Day 1 of adulthood (YA). Worm pellets were resuspended in 50ul RIPA buffer lysate (2%SDS) supplemented with a protease inhibitor cocktail tablet. Worm pellets were flash frozen in liquid nitrogen and crushed (4 cycles) in microcentrifuge tubes using a plastic dounce homogenizer. Lysates were then heated at 95˚ C for 10 mintues. Protein concentration in each sample was estimated using the PierceTM BCA Protein Assay Kit (Thermo Scientific) following the instructions of the manufacturer.

The collected worm lysate was boiled in lysis buffer (5% sodium dodecyl sulfate (SDS), 5 mm tris(2-carboxyethyl)phosphine (TCEP), 10 mm chloroacetamide (CAA), 100 mm Tris, pH 8.5) for 10 min followed by micro tip probe sonication (Q705 Sonicator from Fisherbrand) for 2 min with pulses of 1s on and 1s off at 80% amplitude. Protein concentration was estimated by NanoDrop (Thermo Fisher

Scientific). Protein digestion was automated on a KingFisher APEX robot (Thermo Fisher Scientific) in 96-well format using a protocol from Bekker-Jensen at al [66] with some modifications. The 96-well comb is stored in plate #1, the sample in plate #2 in a final concentration of 70% acetonitrile and with magnetic MagReSyn Hydroxyl beads (ReSyn Biosciences) in a protein/bead ratio of 1:2. Washing solutions are in plates #3–5 (95% Acetonitrile (ACN)) and plates #6–7 (70% Ethanol). Plate #8 contains 300 µL digestion solution of 100 mm Tris pH 8.5 and trypsin (Promega) in an enzyme:protein ratio of 1:100. The protein aggregation was carried out in two steps of 1 min mixing at medium mixing speed, followed by a 10 min pause each. The sequential washes were performed in 2.5 min and slow speed, without releasing the beads from the magnet. The digestion was set to 12 h at 37 degrees with slow speed. Protease activity was quenched by acidification with trifluoroacetic acid (TFA) to a final ph of 2, and the resulting peptide mixture was purified on OASIS HLB 96 wellplate (Waters). Peptides were eluted twice with 100µL of 50% ACN and dried in a Savant DNA120 (Thermo Fisher Scientific).

Peptides were then dissolved in 2% formic acid before liquid chromatography–tandem mass spectrometry (MS/MS) analysis. The mixture of tryptic peptides was analysed using an Ultimate3000 high-performance liquid chromatography system coupled online to an Eclipse mass spectrometer (Thermo Fisher Scientific). Buffer A consisted of water acidified with 0.1% formic acid, while buffer B was 80% acetonitrile and 20% water with 0.1% formic acid. The peptides were first trapped for 1 min at 30 µl/min with 100% buffer A on a trap (0.3 mm by 5 mm with PepMap C18, 5 µm, 100 Å; Thermo Fisher Scientific); after trapping, the peptides were separated by a 50-cm analytical column (Acclaim PepMap, 3 µm; Thermo Fisher Scientific). The gradient was 7 to 35% B in 103 min at 300 nl/min. Buffer B was then raised to 55% in 3 min and increased to 99% for the cleaning step. Peptides were ionized using a spray voltage of 2.1 kV and a capillary heated at 280°C. The mass spectrometer was set to acquire full-scan MS spectra (350 to 1400 mass/charge ratio) for a maximum injection time set to Auto at a mass resolution of 60,000 and an automated gain control (AGC) target value of 100%. For MSMS fragmentation we chose the DIA approach: AGC target value for fragment spectra was set at 200%. 60 windows of 10 Da were used with an overlap of 1 Da (m/z range from 380 to 980). Resolution was set to 15,000 and IT to 40 ms. Normalized collision energy was set at 30%. All raw files were analysed by DIA-NN v1.8.1 [67], searching against library generated automatically using *C. elegans* proteome (downloaded from UniProt) and standard settings: peptides from 7 to 30 AA, max number of missed cleavages of 1, oxidation (M) and protein-Acetylation as only variable modifications.

The data analysis was performed using Perseus software platform. Briefly, the original data was first log2 transformed and then only the proteins with at least 3 values from the 4 reps were kept. At this point the missing data were imputed using automatic settings of Perseus. The imputed data was then analysed on Perseus platform by generating a volcano plot analysis to view the differential protein expression between genetic backgrounds being compared. FDR of 0.05 was applied as cut-off and for each protein, significance is shown as $-\text{Log}_{10}$(p-value) coming from the t-test, as the difference between backgrounds compared.

The mass spectrometry proteomics data have been deposited to the ProteomeXchange Consortium via the PRIDE [68] partner repository with the dataset identifier PXD044595.

Relative mtDNA content

mtDNA content relative to nuclear DNA in worms was quantified using 7 single Day 1 (YA) worms from wildtype, *ubql-1(tm1574)*, *hsf-1* OE and *hsf-1* OE;*ubql-1(tm1574)* worm populations cultured on OP50 bacteria. Each single worm was added to 10ul worm lysis buffer containing proteinase K and flash frozen in liquid nitrogen. For standards, 5 Day1 (YA) worms from each background were collected in the same way as described earlier. All samples were incubated at 65°C for 90 mins, then at 95°C for 15 min to release genomic DNA. Primers for nuclear gene *cdc-42p* and a mitochondrial gene *nd-1* were used to estimate nuclear and mitochondrial DNA content. Quantitative PCR was performed using Biorad CFX96 Real-time PCR detection system and BioRad SsoAdvanced SYBR green super mix. Quantification of relative gene expression of mtDNA:nuclearDNA was performed with the standard curve method.

Quantification and statistical analysis

Sample number (n) corresponds to the number of biological replicates/trials or number of animals used, as stated in each figure legend. In all cases, error bars correspond to SD. All statistical tests (log rank (Mantel-Cox), one-way ANOVA) were carried out as stated within each figure legend using GraphPad Prism 10. The statistical details of all experiments can be found within the accompanying figure legends.

Declarations

Acknowledgements

We thank members of the Labbadia lab and UCL Institute of Healthy Ageing for helpful discussions regarding the manuscript. We also thank the Biosciences Molecular Biology Facility for use of core equipment and Novogene UK for cDNA library preparation and RNA-sequencing.

Funding

J.L., X.W., R.W. and A.P.E. were funded by BBSRC grant BB/T013273/1. K.T. was funded by a Wellcome Collaborative Award in Science (209250/Z/17/Z). The Mass spectrometry instrumentation was funded by a Wellcome Trust Multiuser Equipment grant (221521/Z/20/Z) to K.T.

Author contributions

A.P.E., X.W. and R.W. performed all experiments with the exception of mass-spectrometry based proteomics, which were performed by R.Z.C. All data were analysed by A.P.E. and R.Z.C. with supervision from J.L. and K.T. J.L., A.P.E., R.Z.C. and K.T. made all figures and wrote the manuscript.

Competing Interests

The authors have no competing interests to declare.

Data and Materials Availability

All data are provided within the manuscript with the exception of RNA-seq and mass-spec data, which can be accessed using the accession numbers provided in the Materials and Methods.

References

1. Lopez-Otin, C., Blasco, M. A., Partridge, L., Serrano, M. & Kroemer, G. Hallmarks of aging: An expanding universe. *Cell* **186**, 243-278 (2023). https://doi.org:10.1016/j.cell.2022.11.001
2. Douglas, P. M. & Dillin, A. Protein homeostasis and aging in neurodegeneration. *J Cell Biol* **190**, 719-729 (2010). https://doi.org:10.1083/jcb.201005144
3. Labbadia, J. & Morimoto, R. I. The biology of proteostasis in aging and disease. *Annu Rev Biochem* **84**, 435-464 (2015). https://doi.org:10.1146/annurev-biochem-060614-033955
4. Akerfelt, M., Morimoto, R. I. & Sistonen, L. Heat shock factors: integrators of cell stress, development and lifespan. *Nat Rev Mol Cell Biol* **11**, 545-555 (2010). https://doi.org:10.1038/nrm2938
5. Li, J., Labbadia, J. & Morimoto, R. I. Rethinking HSF1 in Stress, Development, and Organismal Health. *Trends Cell Biol* **27**, 895-905 (2017). https://doi.org:10.1016/j.tcb.2017.08.002
6. Brunquell, J., Morris, S., Lu, Y., Cheng, F. & Westerheide, S. D. The genome-wide role of HSF-1 in the regulation of gene expression in Caenorhabditis elegans. *BMC Genomics* **17**, 559 (2016). https://doi.org:10.1186/s12864-016-2837-5
7. Kumsta, C., Chang, J. T., Schmalz, J. & Hansen, M. Hormetic heat stress and HSF-1 induce autophagy to improve survival and proteostasis in C. elegans. *Nat Commun* **8**, 14337 (2017). https://doi.org:10.1038/ncomms14337
8. Watterson, A. *et al.* Loss of heat shock factor initiates intracellular lipid surveillance by actin destabilization. *Cell Rep* **41**, 111493 (2022). https://doi.org:10.1016/j.celrep.2022.111493
9. Baird, N. A. *et al.* HSF-1-mediated cytoskeletal integrity determines thermotolerance and life span. *Science* **346**, 360-363 (2014). https://doi.org:10.1126/science.1253168
10. Mah, A. L., Perry, G., Smith, M. A. & Monteiro, M. J. Identification of ubiquilin, a novel presenilin interactor that increases presenilin protein accumulation. *J Cell Biol* **151**, 847-862 (2000). https://doi.org:10.1083/jcb.151.4.847
11. Ko, H. S., Uehara, T., Tsuruma, K. & Nomura, Y. Ubiquilin interacts with ubiquitylated proteins and proteasome through its ubiquitin-associated and ubiquitin-like domains. *FEBS Lett* **566**, 110-114 (2004). https://doi.org:10.1016/j.febslet.2004.04.031
12. Hsu, A. L., Murphy, C. T. & Kenyon, C. Regulation of aging and age-related disease by DAF-16 and heat-shock factor. *Science* **300**, 1142-1145 (2003). https://doi.org:10.1126/science.1083701
13. Morley, J. F. & Morimoto, R. I. Regulation of longevity in Caenorhabditis elegans by heat shock factor and molecular chaperones. *Mol Biol Cell* **15**, 657-664 (2004). https://doi.org:10.1091/mbc.e03-07-

0532

14. Li, J., Chauve, L., Phelps, G., Brielmann, R. M. & Morimoto, R. I. E2F coregulates an essential HSF developmental program that is distinct from the heat-shock response. *Genes Dev* **30**, 2062-2075 (2016). https://doi.org:10.1101/gad.283317.116
15. Morley, J. F., Brignull, H. R., Weyers, J. J. & Morimoto, R. I. The threshold for polyglutamine-expansion protein aggregation and cellular toxicity is dynamic and influenced by aging in Caenorhabditis elegans. *Proc Natl Acad Sci U S A* **99**, 10417-10422 (2002). https://doi.org:10.1073/pnas.152161099
16. Prahlad, V. & Morimoto, R. I. Neuronal circuitry regulates the response of Caenorhabditis elegans to misfolded proteins. *Proc Natl Acad Sci U S A* **108**, 14204-14209 (2011). https://doi.org:10.1073/pnas.1106557108
17. Raudvere, U. *et al.* g:Profiler: a web server for functional enrichment analysis and conversions of gene lists (2019 update). *Nucleic Acids Res* **47**, W191-W198 (2019). https://doi.org:10.1093/nar/gkz369
18. Watterson, A. *et al.* Intracellular lipid surveillance by small G protein geranylgeranylation. *Nature* **605**, 736-740 (2022). https://doi.org:10.1038/s41586-022-04729-7
19. Van Gilst, M. R., Hadjivassiliou, H., Jolly, A. & Yamamoto, K. R. Nuclear hormone receptor NHR-49 controls fat consumption and fatty acid composition in C. elegans. *PLoS Biol* **3**, e53 (2005). https://doi.org:10.1371/journal.pbio.0030053
20. Ratnappan, R. *et al.* Germline signals deploy NHR-49 to modulate fatty-acid beta-oxidation and desaturation in somatic tissues of C. elegans. *PLoS Genet* **10**, e1004829 (2014). https://doi.org:10.1371/journal.pgen.1004829
21. Van Gilst, M. R., Hadjivassiliou, H. & Yamamoto, K. R. A Caenorhabditis elegans nutrient response system partially dependent on nuclear receptor NHR-49. *Proc Natl Acad Sci U S A* **102**, 13496-13501 (2005). https://doi.org:10.1073/pnas.0506234102
22. Tanaka, T. *et al.* Activation of peroxisome proliferator-activated receptor delta induces fatty acid beta-oxidation in skeletal muscle and attenuates metabolic syndrome. *Proc Natl Acad Sci U S A* **100**, 15924-15929 (2003). https://doi.org:10.1073/pnas.0306981100
23. Pathare, P. P., Lin, A., Bornfeldt, K. E., Taubert, S. & Van Gilst, M. R. Coordinate regulation of lipid metabolism by novel nuclear receptor partnerships. *PLoS Genet* **8**, e1002645 (2012). https://doi.org:10.1371/journal.pgen.1002645
24. Itakura, E. *et al.* Ubiquilins Chaperone and Triage Mitochondrial Membrane Proteins for Degradation. *Mol Cell* **63**, 21-33 (2016). https://doi.org:10.1016/j.molcel.2016.05.020
25. Lim, P. J. *et al.* Ubiquilin and p97/VCP bind erasin, forming a complex involved in ERAD. *J Cell Biol* **187**, 201-217 (2009). https://doi.org:10.1083/jcb.200903024
26. Whiteley, A. M. *et al.* Ubiquilin1 promotes antigen-receptor mediated proliferation by eliminating mislocalized mitochondrial proteins. *Elife* **6** (2017). https://doi.org:10.7554/eLife.26435
27. Franz, A., Ackermann, L. & Hoppe, T. Create and preserve: proteostasis in development and aging is governed by Cdc48/p97/VCP. *Biochim Biophys Acta* **1843**, 205-215 (2014).

https://doi.org:10.1016/j.bbamcr.2013.03.031

28. Benedetti, C., Haynes, C. M., Yang, Y., Harding, H. P. & Ron, D. Ubiquitin-like protein 5 positively regulates chaperone gene expression in the mitochondrial unfolded protein response. *Genetics* **174**, 229-239 (2006). https://doi.org:10.1534/genetics.106.061580
29. Wahlby, C. *et al.* High- and low-throughput scoring of fat mass and body fat distribution in C. elegans. *Methods* **68**, 492-499 (2014) https://doi.org:10.1016/j.ymeth.2014.04.017
30. Nunnari, J. & Suomalainen, A. Mitochondria: in sickness and in health. *Cell* **148**, 1145-1159 (2012). https://doi.org:10.1016/j.cell.2012.02.035
31. Youle, R. J. & van der Bliek, A. M. Mitochondrial fission, fusion, and stress. *Science* **337**, 1062-1065 (2012). https://doi.org:10.1126/science.1219855
32. Weir, H. J. *et al.* Dietary Restriction and AMPK Increase Lifespan via Mitochondrial Network and Peroxisome Remodeling. *Cell Metab* **26**, 884-896 e885 (2017). https://doi.org:10.1016/j.cmet.2017.09.024
33. Labrousse, A. M., Zappaterra, M. D., Rube, D. A. & van der Bliek, A. M. C. elegans dynamin-related protein DRP-1 controls severing of the mitochondrial outer membrane. *Mol Cell* **4**, 815-826 (1999). https://doi.org:10.1016/s1097-2765(00)80391-3
34. Ichishita, R. *et al.* An RNAi screen for mitochondrial proteins required to maintain the morphology of the organelle in Caenorhabditis elegans. *J Biochem* **143**, 449-454 (2008). https://doi.org:10.1093/jb/mvm245
35. Kanazawa, T. *et al.* The C. elegans Opa1 homologue EAT-3 is essential for resistance to free radicals. *PLoS Genet* **4**, e1000022 (2008). https://doi.org:10.1371/journal.pgen.1000022
36. Twig, G. *et al.* Fission and selective fusion govern mitochondrial segregation and elimination by autophagy. *EMBO J* **27**, 433-446 (2008). https://doi.org:10.1038/sj.emboj.7601963
37. Zheng, T., Yang, Y. & Castaneda, C. A. Structure, dynamics and functions of UBQLNs: at the crossroads of protein quality control machinery. *Biochem J* **477**, 3471-3497 (2020). https://doi.org:10.1042/BCJ20190497
38. Lin, B. C., Higgins, N. R., Phung, T. H. & Monteiro, M. J. UBQLN proteins in health and disease with a focus on UBQLN2 in ALS/FTD. *FEBS J* **289**, 6132-6153 (2022). https://doi.org:10.1111/febs.16129
39. Kim, T. Y., Kim, E., Yoon, S. K. & Yoon, J. B. Herp enhances ER-associated protein degradation by recruiting ubiquilins. *Biochem Biophys Res Commun* **369**, 741-746 (2008). https://doi.org:10.1016/j.bbrc.2008.02.086
40. Hirayama, S. *et al.* Nuclear export of ubiquitinated proteins via the UBIN-POST system. *Proc Natl Acad Sci U S A* **115**, E4199-E4208 (2018). https://doi.org:10.1073/pnas.1711017115
41. Sural, S., Liang, C. Y., Wang, F. Y., Ching, T. T. & Hsu, A. L. HSB-1/HSF-1 pathway modulates histone H4 in mitochondria to control mtDNA transcription and longevity. *Sci Adv* **6** (2020). https://doi.org:10.1126/sciadv.aaz4452

42. Sala, A. J. *et al.* Nuclear receptor signaling via NHR-49/MDT-15 regulates stress resilience and proteostasis in response to reproductive and metabolic cues. *bioRxiv* (2023). https://doi.org:10.1101/2023.04.25.537803
43. Oleson, B. *et al.* Early life changes in histone landscape protect against age-associated amyloid toxicities through HSF-1 dependent regulation of lipid metabolism. (2023).
44. Wong, Y. C., Kim, S., Peng, W. & Krainc, D. Regulation and Function of Mitochondria-Lysosome Membrane Contact Sites in Cellular Homeostasis. *Trends Cell Biol* **29**, 500-513 (2019). https://doi.org:10.1016/j.tcb.2019.02.004
45. Folick, A. *et al.* Aging. Lysosomal signaling molecules regulate longevity in Caenorhabditis elegans. *Science* **347**, 83-86 (2015). https://doi.org:10.1126/science.1258857
46. Ramachandran, P. V. *et al.* Lysosomal Signaling Promotes Longevity by Adjusting Mitochondrial Activity. *Dev Cell* **48**, 685-696 e685 (2019). https://doi.org:10.1016/j.devcel.2018.12.022
47. Sun, Y. *et al.* Lysosome activity is modulated by multiple longevity pathways and is important for lifespan extension in C. elegans. *Elife* **9** (2020). https://doi.org:10.7554/eLife.55745
48. Sharma, A., Smith, H. J., Yao, P. & Mair, W. B. Causal roles of mitochondrial dynamics in longevity and healthy aging. *EMBO Rep* **20**, e48395 (2019). https://doi.org:10.15252/embr.201948395
49. Westermann, B. Bioenergetic role of mitochondrial fusion and fission. *Biochim Biophys Acta* **1817**, 1833-1838 (2012). https://doi.org:10.1016/j.bbabio.2012.02.033
50. Chen, H., Chomyn, A. & Chan, D. C. Disruption of fusion results in mitochondrial heterogeneity and dysfunction. *J Biol Chem* **280**, 26185-26192 (2005). https://doi.org:10.1074/jbc.M503062200
51. Olichon, A. *et al.* Loss of OPA1 perturbates the mitochondrial inner membrane structure and integrity, leading to cytochrome c release and apoptosis. *J Biol Chem* **278**, 7743-7746 (2003). https://doi.org:10.1074/jbc.C200677200
52. Trevisan, T. *et al.* Manipulation of Mitochondria Dynamics Reveals Separate Roles for Form and Function in Mitochondria Distribution. *Cell Rep* **23**, 1742-1753 (2018). https://doi.org:10.1016/j.celrep.2018.04.017
53. Shah, P. P. *et al.* Ubiquilin1 represses migration and epithelial-to-mesenchymal transition of human non-small cell lung cancer cells. *Oncogene* **34**, 1709-1717 (2015). https://doi.org:10.1038/onc.2014.97
54. Etienne-Manneville, S. & Hall, A. Rho GTPases in cell biology. *Nature* **420**, 629-635 (2002). https://doi.org:10.1038/nature01148
55. Higuchi-Sanabria, R. *et al.* Spatial regulation of the actin cytoskeleton by HSF-1 during aging. *Mol Biol Cell* **29**, 2522-2527 (2018). https://doi.org:10.1091/mbc.E18-06-0362
56. Sing, C. N. *et al.* Identification of a modulator of the actin cytoskeleton, mitochondria, nutrient metabolism and lifespan in yeast. *Nat Commun* **13**, 2706 (2022). https://doi.org:10.1038/s41467-022-30045-9

57. Higuchi, R. *et al.* Actin dynamics affect mitochondrial quality control and aging in budding yeast. *Curr Biol* **23**, 2417-2422 (2013). https://doi.org:10.1016/j.cub.2013.10.022
58. Illescas, M., Penas, A., Arenas, J., Martin, M. A. & Ugalde, C. Regulation of Mitochondrial Function by the Actin Cytoskeleton. *Front Cell Dev Biol* **9**, 795838 (2021). https://doi.org:10.3389/fcell.2021.795838
59. Shah, M., Chacko, L. A., Joseph, J. P. & Ananthanarayanan, V. Mitochondrial dynamics, positioning and function mediated by cytoskeletal interactions. *Cell Mol Life Sci* **78**, 3969-3986 (2021). https://doi.org:10.1007/s00018-021-03762-5
60. Pernas, L. & Scorrano, L. Mito-Morphosis: Mitochondrial Fusion, Fission, and Cristae Remodeling as Key Mediators of Cellular Function. *Annu Rev Physiol* **78**, 505-531 (2016). https://doi.org:10.1146/annurev-physiol-021115-105011
61. Brenner, S. The genetics of Caenorhabditis elegans. *Genetics* **77**, 71-94 (1974). https://doi.org:10.1093/genetics/77.1.71
62. Kamath, R. S. *et al.* Systematic functional analysis of the Caenorhabditis elegans genome using RNAi. *Nature* **421**, 231-237 (2003). https://doi.org:10.1038/nature01278
63. Herndon, L. A. *et al.* Stochastic and genetic factors influence tissue-specific decline in ageing C. elegans. *Nature* **419**, 808-814 (2002). https://doi.org:10.1038/nature01135
64. Goedhart, J. & Luijsterburg, M. S. VolcaNoseR is a web app for creating, exploring, labeling and sharing volcano plots. *Sci Rep* **10**, 20560 (2020). https://doi.org:10.1038/s41598-020-76603-3
65. Koopman, M. *et al.* A screening-based platform for the assessment of cellular respiration in Caenorhabditis elegans. *Nat Protoc* **11**, 1798-1816 (2016). https://doi.org:10.1038/nprot.2016.106
66. Bekker-Jensen, D. B. *et al.* A Compact Quadrupole-Orbitrap Mass Spectrometer with FAIMS Interface Improves Proteome Coverage in Short LC Gradients. *Mol Cell Proteomics* **19**, 716-729 (2020). https://doi.org:10.1074/mcp.TIR119.001906
67. Demichev, V., Messner, C. B., Vernardis, S. I., Lilley, K. S. & Ralser, M. DIA-NN: neural networks and interference correction enable deep proteome coverage in high throughput. *Nat Methods* **17**, 41-44 (2020). https://doi.org:10.1038/s41592-019-0638-x
68. Perez-Riverol, Y. *et al.* The PRIDE database resources in 2022: a hub for mass spectrometry-based proteomics evidences. *Nucleic Acids Res* **50**, D543-D552 (2022). https://doi.org:10.1093/nar/gkab1038

Figures

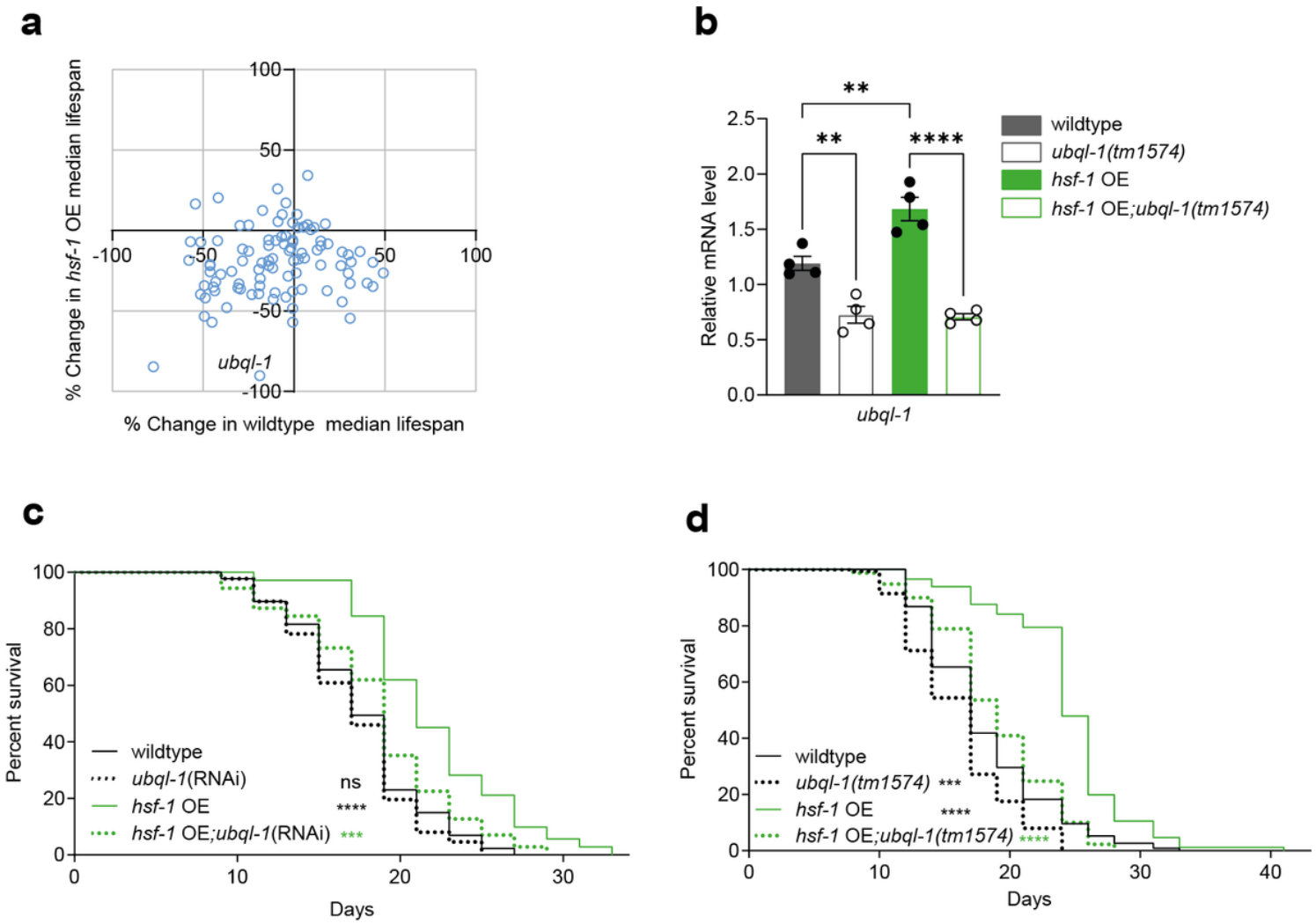

Figure 1

Ubiquilin-1 is necessary for *hsf-1* OE to extend lifespan

(a) Changes in median lifespan in wildtype and *hsf-1* overexpressing (*hsf-1* OE) worms after RNAi against HSF-1 target genes (n ≥ 40 animals per group) **(b)** Relative expression of *ubql-1* mRNA on day 1 of adulthood in wildtype, *ubql-1(tm1574)*, *hsf-1* OE, and *hsf-1* OE; *ubql-1(tm1574)* animals grown on OP50. Data are the mean of 4 biological replicates. **(c-d)** Lifespan of **(c)** wildtype and *hsf-1* OE animals on empty vector and *ubql-1*(RNAi) and **(d)** wildtype, *ubql-1(tm1574)*, *hsf-1* OE, *hsf-1* OE;*ubql-1(tm1574)* animals grown on OP50. All error bars denote SD. Statistical significance was calculated using One-way ANOVA with post-analysis pairwise comparison of groups **(b)** and the Mantel-Cox log rank test **(c-d)**. ns, not significant ($p > 0.05$), **$p < 0.01$, ***$p < 0.001$, ****$p<0.0001$. Full statistics for lifespan trials (including n values) can be found in Supplementary Table 2.

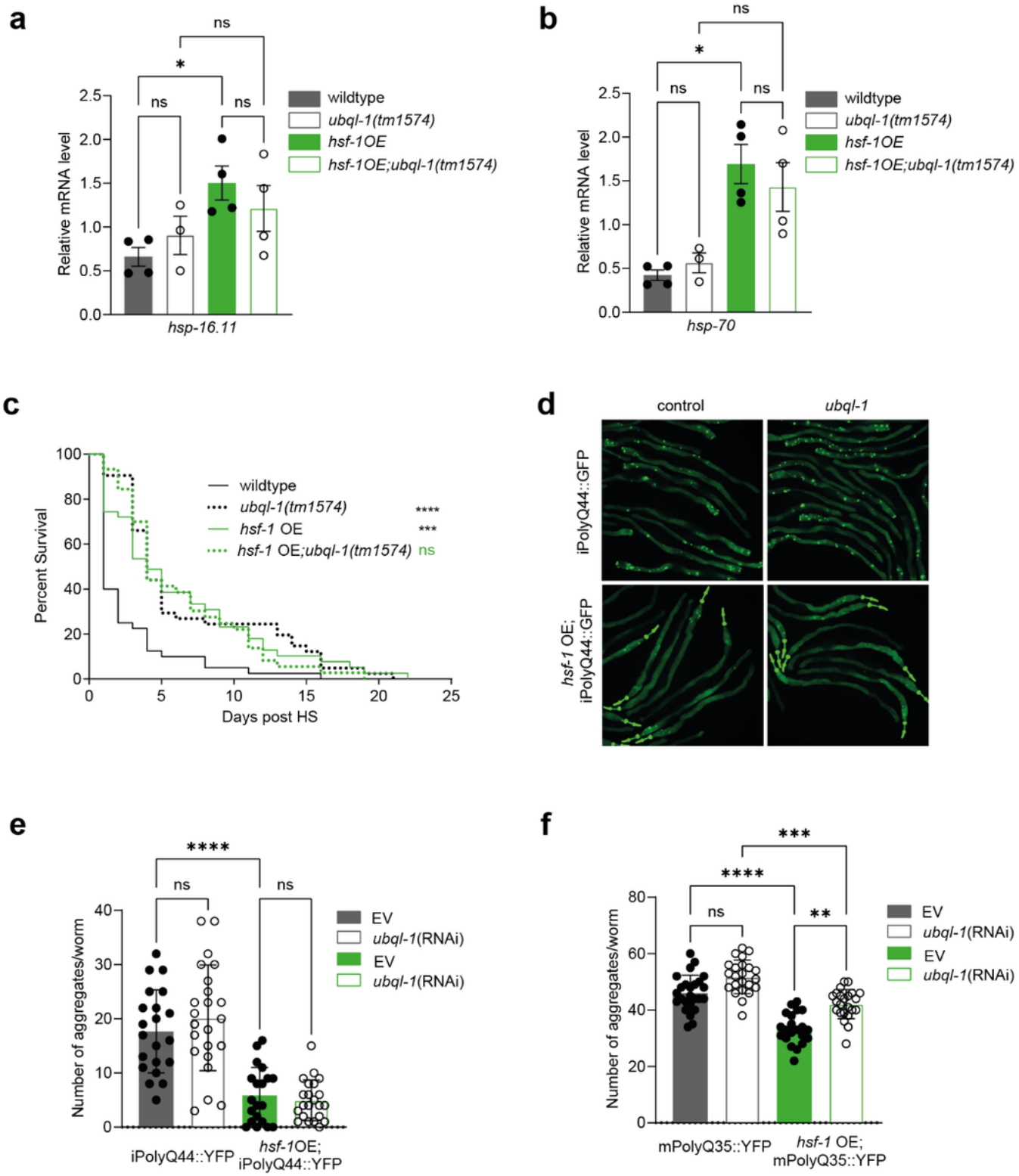

Figure 2

Ubiquilin-1 is not necessary for enhanced proteostasis capacity

(a-b) Relative expression of *hsp-16.11* and *hsp-70* mRNA on day 1 of adulthood in wildtype, *ubql-1(tm1574)*, *hsf-1* OE, and *hsf-1* OE;*ubql-1(tm1574)* animals grown on OP50 and subjected to heat shock (33˚C, 30 mins). Data are the mean of 4 biological replicates. **(c)** Survival of wildtype, *ubql-1(tm1574)*,

hsf-1 OE, *hsf-1* OE;*ubql-1(tm1574)* animals on D1 of adulthood following exposure to heat shock (35˚C for 4 h) **(d)** Representative images of wildtype and *hsf-1* OE worms expressing intestinal polyQ44::YFP grown on empty vector or *ubql-1*(RNAi) at day 5 of adulthood. **(e-f)** Number of polyglutamine::YFP aggregates present in the **(e)** intestine (Q44::YFP) and **(f)** body wall muscle (Q35::YFP) on D5 of adulthood in wildtype and *hsf-1* OE animals grown on empty vector and *ubql-1*(RNAi). One of two independent experiments has been represented for intestinal and muscle PolyQ sensors. Between 20-25 worms were mounted to assess PolyQ::YFP aggregates in intestine and muscle. All error bars denote SD. Statistical significance was calculated using One-way ANOVA with post-analysis pairwise comparison of groups **(a,b,e,f)** and the Mantel-Cox log rank test **(c)**. ns, not significant ($p>0.05$), *$p<0.05$, **$p < 0.01$, ***$p < 0.001$, ****$p<0.0001$. Full statistics for lifespan trials (including n values) can be found in Supplementary Table 2.

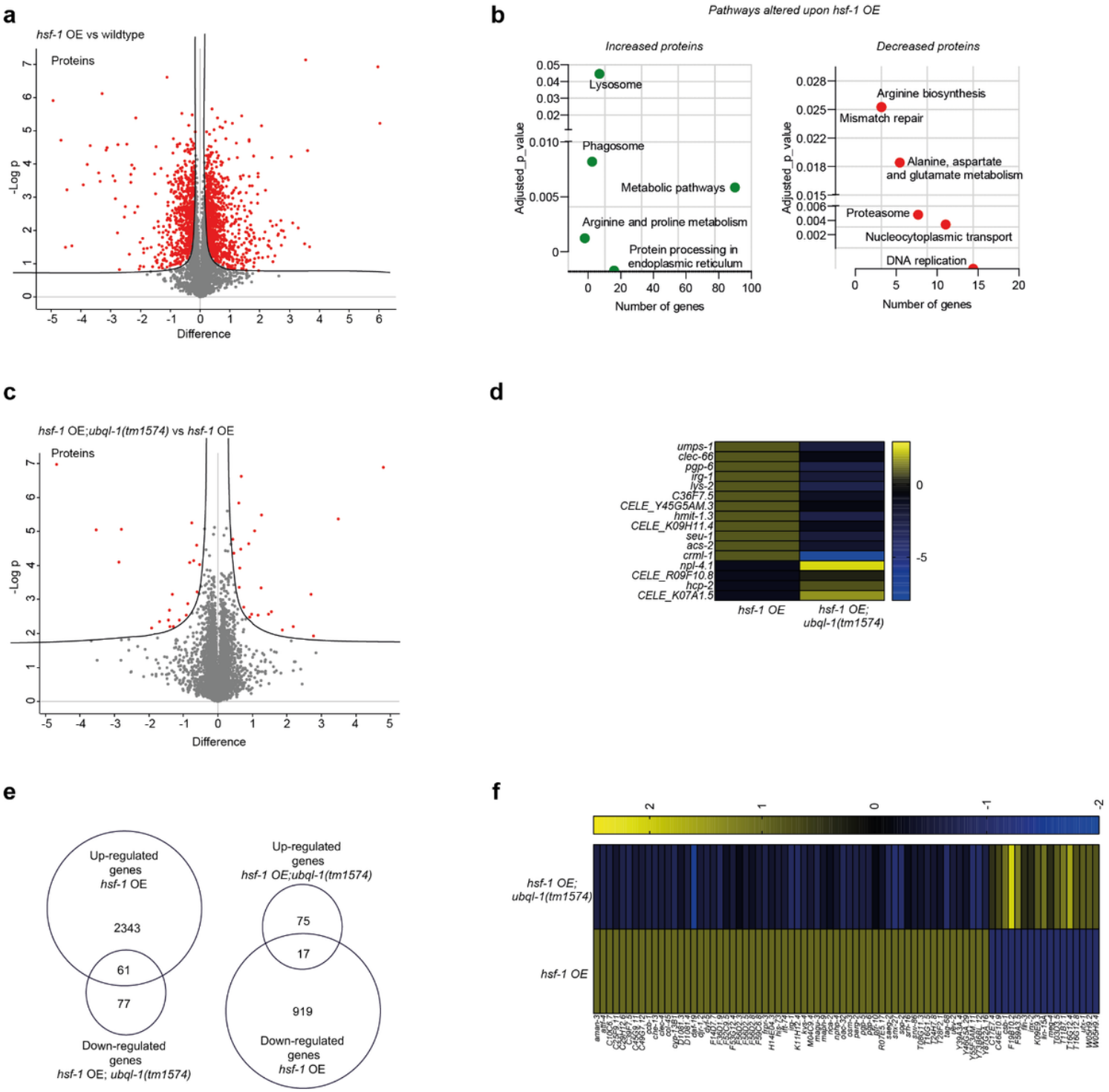

Figure 3

Ubiquilin-1 is necessary for metabolic re-wiring in *hsf-1* OE animals

(a,c) Volcano plots representing differentially expressed proteins (red dots) between the groups tested, **(a)** *hsf-1* OE *vs* wildtype worms and **(c)** *hsf-1* OE; *ubql-1(tm1574) vs hsf-1* OE collected at Day1 of adulthood. Red dots in the right and left region of each volcano plot represent proteins significantly up-regulated and down-regulated. 4 biological replicates per genetic background were assessed during Proteomics analyses **(b)** KEGG pathway enrichment analysis of the significantly up-regulated (left) and

downregulated (right) proteins upon *hsf-1* overexpression.**(d)** Heatmap of UBQL-1 dependent changes in protein abundance in *hsf-1* OE worms. **(e)** Venn diagram depicting overlap of significantly up-regulated and downregulated genes altered in a UBQL-1 dependent manner in *hsf-1* OE worms. **(f)** Heatmap depicting the ubiquilin dependent changes in gene expression in *hsf-1* OE worms.

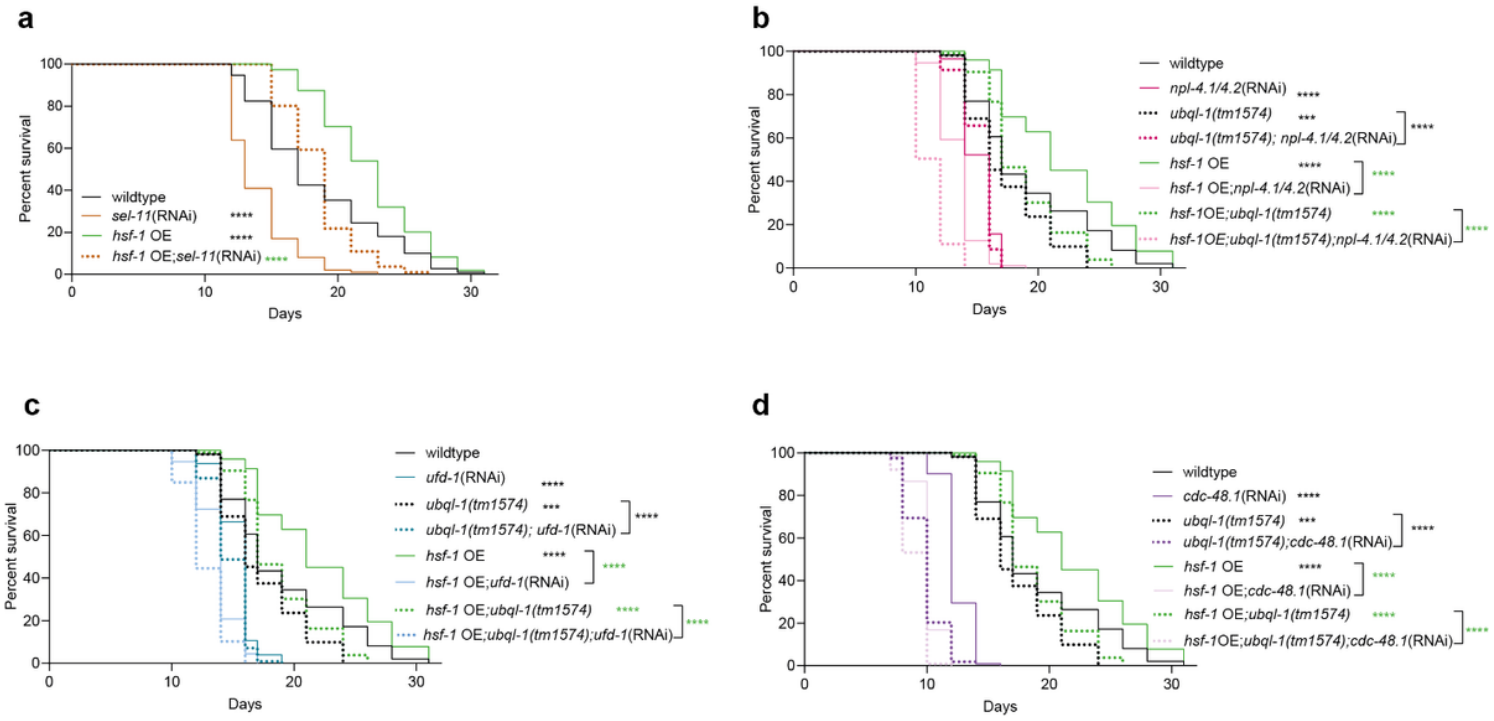

Figure 4

HSF-1-ubiquilin axis requires the CDC48.1/NPL-4.1/UFD-1 complex

(a) Lifespan analysis of wildtype and *hsf-1* OE animals subjected to *sel-11*RNAi. **(b-d)** Lifespan analyses of wildtype, *ubql-1 (tm1574)* mutants, *hsf-1* OE and *hsf-1* OE;*ubql-1(tm1574)* animals subjected to empty vector pL4440 and RNAi-mediated **(b)** *npl-4.1/4.2* (C) *ufd-1*and (d) *cdc-48.1* gene reduction. Statistical significance was calculated using the Mantel-Cox log rank test **(a-d)**. ***p < 0.001, ****p<0.0001. Full statistics for lifespan trials (including n values) can be found in Supplementary Table 2.

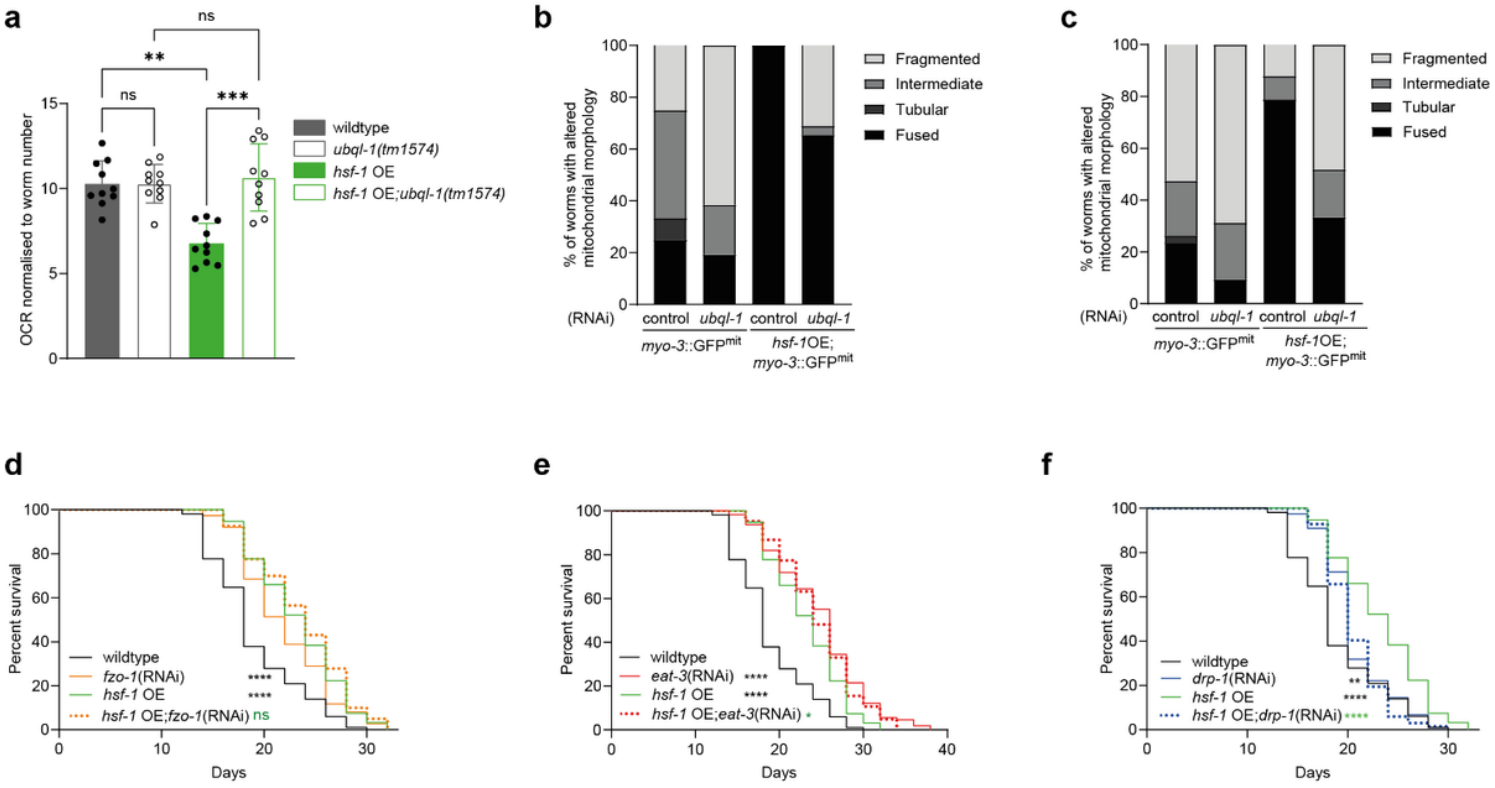

Figure 5

Ubiquilin-1 is necessary for reduced respiration and mitochondrial fusion and disrupting mitochondrial dynamics alters HSF-1 mediated lifespan

(a) Basal Oxygen consumption rates (OCR) in wildtype, *ubql-1(tm1574)*, *hsf-1* OE and *hsf*-1 OE; *ubql-1(tm1574)* animals at Day 1 of adulthood. Mean values (n = 10 replicates per group where each replicate has 10 worms) are plotted. One of two independent experiments has been represented for OCR **(b-c)** Quantification of mitochondrial morphologies in p_{myo-3}::GFP(mit) worms and hsf-1 OE; p_{myo-3}::GFP(mit) worms grown on empty vector control, *ubql-1*(RNAi) on **(b)** Day 2 and **(c)** Day3 adulthood. Refer Supplementary Fig. 5 for additional trial. All error bars denote SD. Statistical significance was calculated by One-Way ANOVA with post-analysis pairwise comparison of groups **(a)**. ns, not significant (p>0.05), **p < 0.01, ***p<0.001. **(d-f)** Lifespan of wildtype and *hsf-1* OE animals on empty vector and **(d)** *fzo-1*(RNAi) (fusion), **(e)** *eat-3* (RNAi) (fusion) and **(f)** *drp-1*(RNAi) (fission). Statistical significance was calculated by Mantel-Cox Log-rank test **(d-f)**. ns, not significant (p>0.05), *p<0.05, **p < 0.01, ****p<0.0001. Full statistics for lifespan trials (including n values) can be found in Supplementary Table 2.

Supplementary Files

This is a list of supplementary files associated with this preprint. Click to download.

- Erinjerietal.2023SupplementaryTable1FINAL.csv

- Erinjerietal.2023SupplementaryTable2FINAL.csv
- Erinjerietal.2023SupplementaryTable3FINAL.csv
- Erinjerietal.2023SupplementaryTable4FINAL.csv
- Erinjerietal.2023SupplementaryTable5FINAL.csv
- ErinjerietalSupplementarymaterials231023.docx
- Accesstodata.docx